Sensitivity of resolved and parameterized surface drag to changes in resolution and parameterization

Article

Accepted Version

van Niekerk, A., Shepherd, T. G., Vosper, S. B. and Webster, S. (2016) Sensitivity of resolved and parameterized surface drag to changes in resolution and parameterization. Quarterly Journal of the Royal Meteorological Society, 142 (699). pp. 2300-2313. ISSN 1477-870X doi: https://doi.org/10.1002/qj.2821 Available at http://centaur.reading.ac.uk/63753/

Sensitivity of resolved and parameterized surface drag to changes in resolution and parameterization

Annelize van Niekerk[a]*, Theodore G. Shepherd[a], Simon B. Vosper[b] and Stuart Webster[b]
[a]*Department of Meteorology, University of Reading, UK*
[b]*Met Office, Exeter, UK*

*Correspondence to: Department of Meteorology, University of Reading, Reading RG6 6BB, UK.
E-mail: a.vanniekerk@pgr.reading.ac.uk

The relative contribution of resolved and parameterized surface drag towards balancing the atmospheric angular momentum flux convergence (AMFC), and their sensitivity to horizontal resolution and parameterization, are investigated in an atmospheric model. This sensitivity can be difficult to elucidate in free-running climate models, in which the AMFC varies with changing climatologies and, as a result, the relative contributions of surface terms balancing the AMFC also vary. While the sensitivity question has previously been addressed using short-range forecasts, we demonstrate that a nudging framework is an effective method for constraining the AMFC. The Met Office Unified Model is integrated at three horizontal resolutions ranging from 130 km (N96) to 25 km (N512) while relaxing the model's wind and temperature fields towards the ERA-interim reanalysis within the altitude regions of maximum AMFC. This method is validated against short range forecasts and good agreement is found. These experiments are then used to assess the fidelity of the exchange between parameterized and resolved orographic torques with changes in horizontal resolution. Although the parameterized orographic torque reduces substantially with increasing horizontal resolution, there is little change in resolved orographic torque over 20N to 50N. The tendencies produced by the nudging routine indicate that the additional drag at lower horizontal resolution is excessive. When parameterized orographic blocking is removed at the coarsest of these resolutions, there is a lack of compensation, and even compensation of the opposite sense, by the boundary layer and resolved torques which is particularly pronounced over 20N to 50N. This study demonstrates that there is strong sensitivity in the behaviour of the resolved and parameterized surface drag over this region.

Key Words: Orographic drag parameterization, angular momentum budget, model resolution, systematic errors, momentum flux, climate model, surface drag

Received . . .

1. Introduction

In general, most of what we have confidence in about the climate response to increased greenhouse gases is understood through thermodynamic arguments and we are left in disagreement over the sensitivity of the atmospheric circulation to climate change (Shepherd 2014). The factors at play are numerous but examination into the way in which modelling centres close their momentum budgets may allow us to attribute some of these dynamical uncertainties to particular processes. One such process that plays a substantial role in the atmospheric momentum budget and varies not only between models but also model resolution is the drag due to orography. This drag arises due to the complex interaction of mountains with the fluid atmosphere. For example, the vertical displacement of air generates gravity waves that can propagate considerable distances in the vertical, acting as an important mechanism for momentum exchange between the surface and upper atmosphere (Teixeira 2014). One such manifestation of this exchange is the role that breaking orographic gravity waves have on sudden stratospheric warmings and the final breakup of the stratospheric polar vortex (McLandress *et al.* 2013). Additionally, when air is not able to ascend topography, it is forced laterally and non-linear behaviour ensues, acting to decelerate the low level flow. Large scale topography also acts as a source of planetary Rossby waves, generating vorticity anomalies due to lifting and vortex stretching or deflection of air from regions of high vorticity to low vorticity (Smith 1979). In particular, the tilt in the upper tropospheric jet is produced by southward deflection of the westerly flow incident on the Rocky Mountains (Brayshaw *et al.* 2009). It is clear that the zonal and hemispheric dynamical asymmetries that we see throughout the atmosphere are shaped by the distribution of orography and without accurate representation of these processes and their role in the momentum budget within models, we are unlikely to produce accurate and robust projections of circulation sensitivity to climate change.

Modelling the influence of orography on the climate system becomes problematic when we are not able to resolve the full orographic spectrum, as we strive for efficiency and battle with computational expense. To atone for this loss of the smaller scales, parameterizations of the sub-grid scale processes are introduced. Their benefits to numerical weather prediction and climate modelling were first recognised by Palmer *et al.* (1986), McFarlane (1987) and Miller *et al.* (1989), who found that excessive westerly wind biases can be alleviated through the addition of a linearly approximated gravity wave drag parameterization. It then became apparent that these sub-grid scale mountain effects went beyond linear gravity wave generation and the addition of a sub-grid scale orographic blocking parameterization, which accounts for the non-linear regimes of flow around orography, led to immense improvements in forecast scores (Lott and Miller 1997; Scinocca and McFarlane 2000; Webster *et al.* 2003).

There are now three orographic effects that are commonly parameterized in global circulation models: the sub-grid scale orographic blocking; gravity wave propagation, which may also include an element of drag due to low-level wave breaking (Scinocca and McFarlane 2000); and turbulent orographic form drag. The first two processes account for scales up to the grid-scale and the turbulent drag accounts for scales at which gravity wave generation becomes impossible, which is taken to be up to approximately 5km (Beljaars *et al.* 2004). However, the separation of drag into these components has led to ambiguity in the size of their respective contributions in the momentum budget. As well as the uncertainty introduced by the various orographic processes, different options for parameterization formulation add another level of complexity. For example, the turbulent orographic form drag can be modelled using an effective roughness length for momentum (Wood and Mason 1993) or through an explicit orographic stress profile (Wood *et al.* 2001; Beljaars *et al.* 2004). The WGNE drag inter-comparison project, which aims to better understand the way in which modelling centres close their momentum budgets, found that the boundary layer stress and low-level orographic blocking parameterizations are often used interchangeably (Zadra *et al.* 2013). The seemingly arbitrary choices of parameters made in parameterization schemes allow for model tuning so that models with lower orographic blocking tended to have higher boundary layer drag, which includes the turbulent orographic form drag parameterization. Since the boundary layer and orographic drag act on different scales and respond to stability in opposite ways, and the boundary layer parameterization has an impact on the energy budget, this compensation of one for the other may be unphysical. What is more, with the growing ethos of seamless atmospheric prediction, in which parameterization schemes are expected to perform well at all resolutions without changing their physics, the exchange between parameterized and resolved orographic drag with increasing resolution may be precarious.

Several studies have assessed the accuracy of orographic drag parameterization schemes over limited area domains using high resolution simulations (Wells *et al.* 2011; Kim and Doyle 2005). Carissimo *et al.* (1988), Clark and Miller (1991) and subsequently Smith *et al.* (2006) looked at the resolution sensitivity of orographic drag over the Alpine regions and found that an increase in resolution did lead to an increase in resolved orographic drag. This is consistent with the notion that an increase in resolution leads to an increase in the height and slope of the Alpine barrier, which, in accordance with orographic drag theory, would lead to non-linear, high drag flow regimes (Nappo 2002; Stein 1992). Additionally, Vosper (2015) showed that a well tuned orographic drag parameterization scheme within an NWP resolution model can reproduce explicitly resolved drag from higher resolution simulations with a good degree of accuracy. In contrast, Brown (2004) investigated the resolution dependence of parameterized and resolved orographic torques in the ECMWF IFS of the time and found that the decrease in the parameterized orographic torque with increased resolution was not compensated by an increase in resolved torque. In fact, the resolved torque changed very little with increasing resolution in certain regions. This leads one to question the ability of models to maintain an equivalent total surface torque across a wide range of resolutions, particularly climate model resolutions.

The attribution of systematic errors can be especially difficult in climate models compared to numerical weather prediction, since we do not have the daily assimilation of data with which to validate the models directly. Comparison of global climate models at different resolutions becomes computationally expensive and problematic when we must produce long time integrations in order to determine model climatology. Even if we are able to compare long time integrations, the feedbacks that act in response to model errors mean that our parameterizations are fed with unrealistic climatological states, making it difficult to disentangle model biases (Phillips *et al.* 2004). Although we may be able to reduce model error at all resolutions as a result of the seamless modelling approach (Martin *et al.* 2010), the errors at lower resolutions may remain large and undetected, leading us into a false sense of security about the quality of our models at lower resolutions. More fundamentally, the model biases addressed in numerical weather prediction, such as mean sea level pressure, may not be as important for climate projections where stratospheric wind biases play an important role (Sigmond and Scinocca 2010).

The drift in short range forecasts has been used in previous studies to evaluate model error (Klinker and Sardeshmukh 1992; Pope and Stratton 2002; Brown 2004): since the model is constrained by initial conditions from observations, this technique is useful for resolution and parameter sensitivity studies. However, performing such analysis can be difficult without access to operational infrastructure. A more accessible means of eliminating model feedbacks and constraining the model climatology is to relax the dynamic and thermodynamic variables towards analysis or reanalysis. Relaxation has been a popular method of diagnosing the influence of certain regions and their teleconnections (Jung 2011; Hoskins *et al.* 2012), as well as being widely used in the chemistry and aerosol community as a method of reproducing the observed meteorological state of the atmosphere (van Aalst *et al.* 2005; Shepherd *et al.* 2014). Spectral nudging has also been used in regional climate modelling to address the problem of lateral boundary condition resolution mis-match, in which only the large scale fields within the RCM are nudged towards the driving GCM (Waldron *et al.* 1996; von Storch *et al.* 2000). This paper seeks to investigate the sensitivity of surface torques to model resolution and parameterization using the nudging approach, in the hope that this will motivate further sensitivity studies and inter-model comparisons employing this method.

The structure of this paper is as follows. Section 2 describes the model setup, nudging sensitivity experiments, analysis and verifications against short range forecasts. The exchange between parameterized and resolved orographic torques with changes in resolution is discussed in section 3. The impact of orographic drag on model bias is discussed in section 4. Section 5 looks at the compensation that occurs between the parameterized orographic torque, the boundary layer torque and resolved orographic torque when blocking is switched off. Finally, conclusions are drawn in section 6.

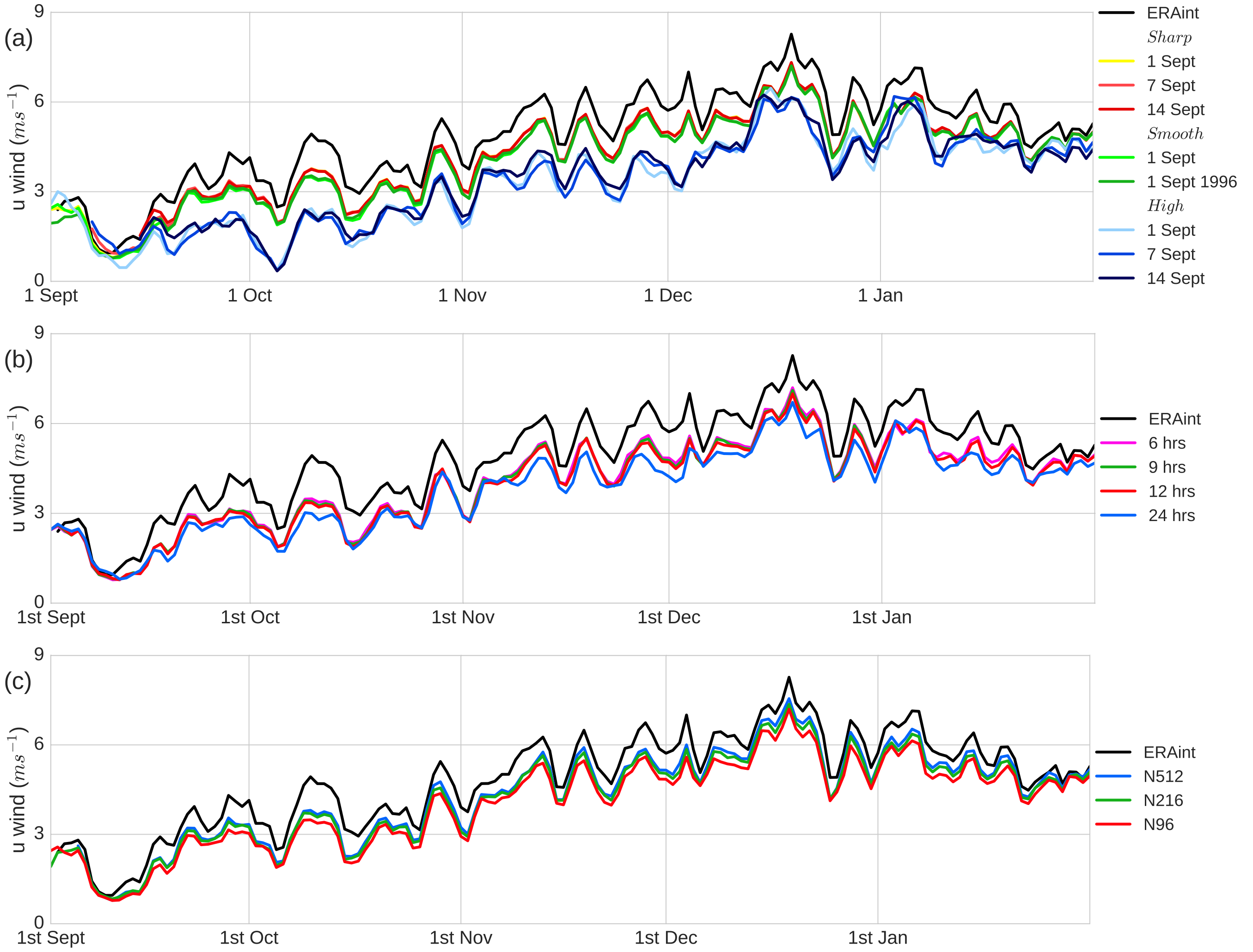

Figure 1. Time-series of the zonal mean zonal wind at 850hPa averaged between 30°N and 50°N over late 1997 and early 1998 for (a) experiments of varying nudging heights and smoothing over model levels initialised from different start dates (see section 2.2), (b) different nudging timescales (τ) and (c) resolutions N96, N216 and N512. In (a) $Sharp$, $Smooth$ and $High$ indicate experiments with smoothing over 2 model levels starting at model level 20, smoothing over 10 model levels starting at model level 20 and smoothing over 10 model levels starting at model level 30, respectively.

2. Methodology

The role of orographic torque in the momentum budget of the atmosphere is investigated using the Met Office Unified Model (MetUM) with the ENDGame dynamical core and Global Atmosphere 6 components integrated at resolutions N96 (130 km), N216 (60 km) and N512 (25 km), all of which have 85 terrain-following vertical levels extending to 85km. The integrations were set up in an AMIP-style configuration with prescribed SSTs and sea-ice concentrations and were initialised from the same N96 initial fields. Details of the orographic blocking and gravity wave drag parameterizations can be found in appendix A of Vosper (2015) and are based on the blocking scheme of Lott and Miller (1997) and gravity wave saturation scheme of McFarlane (1987). As is desirable in a seamless modelling approach, the physics parameters are held constant across all three resolutions with values chosen based on the standard climate and global forecast configurations. The orographic drag parameterization has three free parameters that are poorly constrained by observations: the critical Froude number (set at $F_{crit} = 4$), which determines the amount of blocking such that a higher value leads to increased blocking; the mountain wave amplitude (set at $G = 0.5$); and the flow blocking drag coefficient (set at $C_d = 4$). The parameterization adjusts to the model resolution based on statistical aspects of the sub-grid scale orography, such as the standard deviation, slope and anisotropy, that are recalculated from a 1km resolution dataset at each resolution (Webster *et al.* 2003). As model horizontal resolution increases, the sub-grid orographic standard deviation and slope reduces across the major mountain regions and, since the parameterized orographic blocking and gravity wave drag are proportional to these, the parameterized orographic drag is expected to reduce with increasing resolution.

2.1. Experimental design

The framework of the angular momentum budget is a powerful tool for examining the contribution of surface drag to the large scale structure of the circulation. The vertically integrated, zonally averaged axial component of the relative angular momentum of the atmosphere, $m = ur\cos\phi$, in the non-hydrostatic version of the MetUM is given by (Davies *et al.* 2005):

$$\frac{\partial\left[\int_{z_0}^{\infty} m\rho dz\right]}{\partial t} = -\frac{1}{r\cos\phi}\frac{\partial\left(\left[\int_{z_0}^{\infty} mv\rho dz\right]\cos\phi\right)}{\partial\phi} - \left[\int_{z_0}^{\infty} 2\Omega wr\cos^2\phi\rho dz\right] + \left[\int_{z_0}^{\infty} fvr\cos\phi\rho dz\right] - \left[p_0\frac{\partial z_0}{\partial\lambda}\right] - \left[F_0 r\cos\phi\right] \quad (1)$$

where u is the zonal wind, v is the meridional wind, ρ is the atmospheric density, z_0 is the surface elevation, p_0 is the surface pressure, r is the height dependent radius of the Earth,

ϕ is latitude, Ω is the rate of rotation of the Earth, f is the Coriolis parameter, F_0 is the stress from the parameterized processes and square brackets indicate a zonal average. The terms on the right hand side of the momentum equation are, from left to right: the angular momentum flux convergence (AMFC), which represents the angular momentum being advected into and out of a particular latitude band; the torque due to the non-hydrostatic component of the absolute angular momentum; the torque due to the Coriolis force; the resolved mountain torque (RES); and the parameterized sub-grid scale surface torques. Since the non-hydrostatic component and the Coriolis torque terms are negligible in the steady state limit, the dominant balance in this limit is between the surface terms and the AMFC. By constraining the AMFC at each model resolution through nudging, it is possible to determine the contributions of the resolved and individual parameterized surface terms towards balancing the AMFC.

The model's u, v and T (temperature) fields are relaxed towards the ERA-interim reanalysis variables (Dee *et al.* 2011) on terrain-following model levels within the altitude regions of maximum AMFC (Hartmann 2007), above $\sim$700hPa, while allowing the low level flow to evolve freely. Nudging on terrain-following model levels means that the nudging will be applied at higher altitudes over orography. The nudging is applied through a Newtonian relaxation of the form (Telford *et al.* 2007):

$$X_F^n = X_M^n + \frac{\Delta t}{\tau}(X_A^n - X_M^n) \tag{2}$$

where $X = (u, v, T)$, τ is some relaxation timescale and the superscript n denotes the value at the current time-step. The subscripts are as follows: F denotes that the value is taken as the final variable after nudging; M denotes the variable before nudging but after the model dynamics and physics; and A denotes the variable from the ERA-interim reanalysis. The reanalysis comes from 6 hourly instantaneous values that have been linearly interpolated to the model time-step. The reanalysis data is spatially interpolated from a resolution of $\sim$50 km (N240) to the respective model resolutions using the reconfiguration package within the MetUM.

2.2. *Nudging sensitivity experiments*

If a systematic bias were present in the MetUM relative to the reanalysis, this would require a non-zero time mean zonal mean nudging to be applied within the free atmosphere. In accordance with the downward control principle (Haynes *et al.* 1991), this nudging could induce a meridional circulation extending to the surface below the nudged region and, since the strength of the nudging would change with resolution and parameter settings, the induced circulation and surface flow could also change. This would imply that different model configurations may have different surface flows that are not purely a response to the AMFC alone. Hitchcock and Haynes (2014) showed that the circulation induced from nudging of the zonal mean winds and temperatures was confined within the region of nudging. This alleviates concerns of spurious circulations occurring within the unnudged region in our experimental setup.

Several nudging sensitivity experiments were performed in order to determine appropriate parameter choices, such as the relaxation height, relaxation timescale and spin-up time. The ability of the nudging to constrain the model's low level flow through the AMFC was assessed by varying these parameters and looking at the evolution of the low level zonal winds between 30N and 50N. This region was chosen since it is likely to be the most problematic area for the low-level flow to be constrained as a result of differences in mean orography and parameterized drag across resolutions. The chosen periods for analysis were January 1998 and January 2010, with all nudging sensitivity experiments performed over the January 1998 period. It is worth mentioning that the model wind does not have the exact same amplitude as the ERA-interim wind due to the fact that the model has slightly different topography over this region and, as a result, different pressure levels near the surface. Overall, the low level winds are less sensitive to initial conditions, nudging parameters and nudging height over the Southern Hemisphere (SH) mid-latitudes compared with the Northern Hemisphere (NH) mid-latitudes (not shown) but, as will be shown in the sections to follow, the final nudging parameters chosen give well constrained low-level winds even in the NH mid-latitudes relative to ERA-interim.

Nudging spin-up sensitivity

The spin-up time, initial-condition sensitivity and model drift were tested by initialising from five different start dates of the same free-running model. Figure 1a shows time series of the zonal mean zonal wind at 850hPa averaged between 30N and 50N for experiments with different nudging profiles initialised from the following start dates: the 1st of September 1996 (1 year and 4 months spin up); 1st of September 1997 (4 months spin up); 7th of September 1997 (3 months and 3 weeks spin up); and finally the 14th of September 1997 (3 months and 2 weeks spin up). For nearly all cases, the surface winds responded quite rapidly to the nudging and were very similar to the ERA-interim winds within about 4 days of initialisation. What is more, the longer spin-up period matched the reanalysis winds even after a year, indicating that there is little drift in the nudged model.

Nudging height and smoothing

As a test for imbalances at the nudging boundaries (i.e. regions directly below the nudging height) the smoothing of the nudging over terrain-following model levels was adjusted such that the strength of the nudging was linearly increasing with height over either 10 model levels or 2 model levels, starting at the 20th model level ($\sim$3km or 700hPa). From the vertical structure of the winds and temperatures (not shown), the 10 level smoothing was indistinguishable from the 2 level smoothing. Figure 1a shows the time series of the zonal mean zonal wind at 850hPa averaged between 30N and 50N for the experiments with 10 level smoothing ($Smooth$), and 2 level smoothing ($Sharp$) with different initial conditions. The 10 level smoothing and 2 level smoothing are almost indistinguishable. What is more, they are insensitive to initial conditions and follow the ERA-interim winds well. The 10 level smoothing was chosen due to the fact that the nudging terms were strong at the boundary of the 2 layer smoothing and any sudden discontinuities that may cause spurious imbalances in the model are to be avoided.

The impact of nudging outside of the maximum AMFC region and the sensitivity of the surface winds to this aspect of the nudging was investigated. When applying smoothed nudging starting from the 30th model level ($\sim$7km or 400hPa) to full nudging at the 40th model level ($\sim$12km or 200hPa), the surface winds from ERA-interim were not accurately reproduced. Figure 1a shows that the experiments with nudging started at 7km ($High$) are quite far from those of ERA-interim and show strong sensitivity to initial conditions, since the three ensemble members have varying amplitudes and phase. As a result, the nudging was applied from the 20th model level ($\sim$3km or 700hPa) and smoothed up to the 30th model level ($\sim$7km or 400hPa); this allows for the nudging to be at full strength within the maximum AMFC region.

Nudging timescale sensitivity

The relaxation timescale (τ) was varied between 6 hours, 9 hours, 12 hours and 24 hours. Changing this parameter did not appear to have much of an impact on the evolution of the low-level winds (figure 1b) or the spatial distribution of the nudging tendencies, although the $\tau = 24$ experiment drifts further away from the ERA-interim winds relative to other timescales. A relaxation timescale of 6 hours was chosen to ensure that the model was not able to drift too far from the reanalysis. The sensitivity experiments performed on the MetUM by Telford *et al.* (2007) also suggest that this is the optimal choice for τ, given the temporal frequency of the reanalysis.

2.3. *Momentum budget analysis*

In our analysis of the MetUM momentum budget (eq. 1), the tendency approach to closing the momentum budget was taken, which involves adding together all tendencies that contribute towards the total zonal wind tendency. Since the MetUM uses a semi-Lagrangian upwind advection scheme (Diamantakis *et al.* 2007), it can be problematic to calculate the momentum flux convergence term (first term on RHS of equation 1) in a way that is consistent with the model numerics. As a result, the tendency due to semi-Lagrangian advection was output as 6 hourly instantaneous values on model levels and vertically integrated. It was then possible to deduce the angular momentum flux convergence term as a residual, by subtracting the middle three terms on the RHS of equation 1 from the advection tendency. The non-hydrostatic and Coriolis terms were calculated offline from 6 hourly values of w and v. The resolved mountain torque term was calculated both online and offline using various different methods including calculating the horizontal pressure gradient ($\partial p/\partial\lambda$) and vertically integrating, which, reassuringly, gave the same result as the online calculation. As in Huang and Weickmann (2008), this term was found to be sensitive to the differencing scheme used, and a centred difference scheme calculated online allowed us to close the angular momentum budget to within a negligible amount.

The $F_0 r\cos\phi$ term in equation 1 includes the vertically integrated tendencies from the following parameterizations: the boundary layer turbulent drag (BL); the sub-grid scale orographic drag (SSO), including gravity wave drag and blocking; the spectral gravity wave drag (which integrates to zero at the surface); the convective entrainment of momentum; and the tendencies generated from the nudging routine. All contributions to the $F_0 r\cos\phi$ term were calculated from 6 hourly instantaneous tendencies from parameterizations on 85 model levels.

Figures 2a and 2b show the dominant terms in the angular momentum budget averaged over January 1998 and January 2010 for the three nudged resolution experiments. Each term has been integrated over 10° latitude bands in order to make the resolutions comparable. The solid lines are the values for the N512 experiments and the shading shows the range between the three different resolutions. The width of the shaded region, therefore, indicates the extent of change with resolution of that particular term. The sign of the terms are such that a positive (negative) value contributes towards an acceleration (deceleration) of the atmosphere and a decrease (increase) in the Earth's angular momentum. The magnitude and latitudinal distribution of the terms match closely those of Brown (2004) and Huang *et al.* (1999), although they use a different sign convention. The resolutions used by Brown (2004) are T95, T159, T255 and T511, which corresponds to approximately 210, 125, 80 and 40 km, respectively, making the MetUM N96 and N216 comparable to their T159 and T255. There is disagreement in the sign of the parameterized and resolved torques between 20N and 30N, as was found in their studies, but, unlike them, this is also seen between 10S and 30S in these experiments. This suggests that there are large scale phenomena that impact the resolved pressure

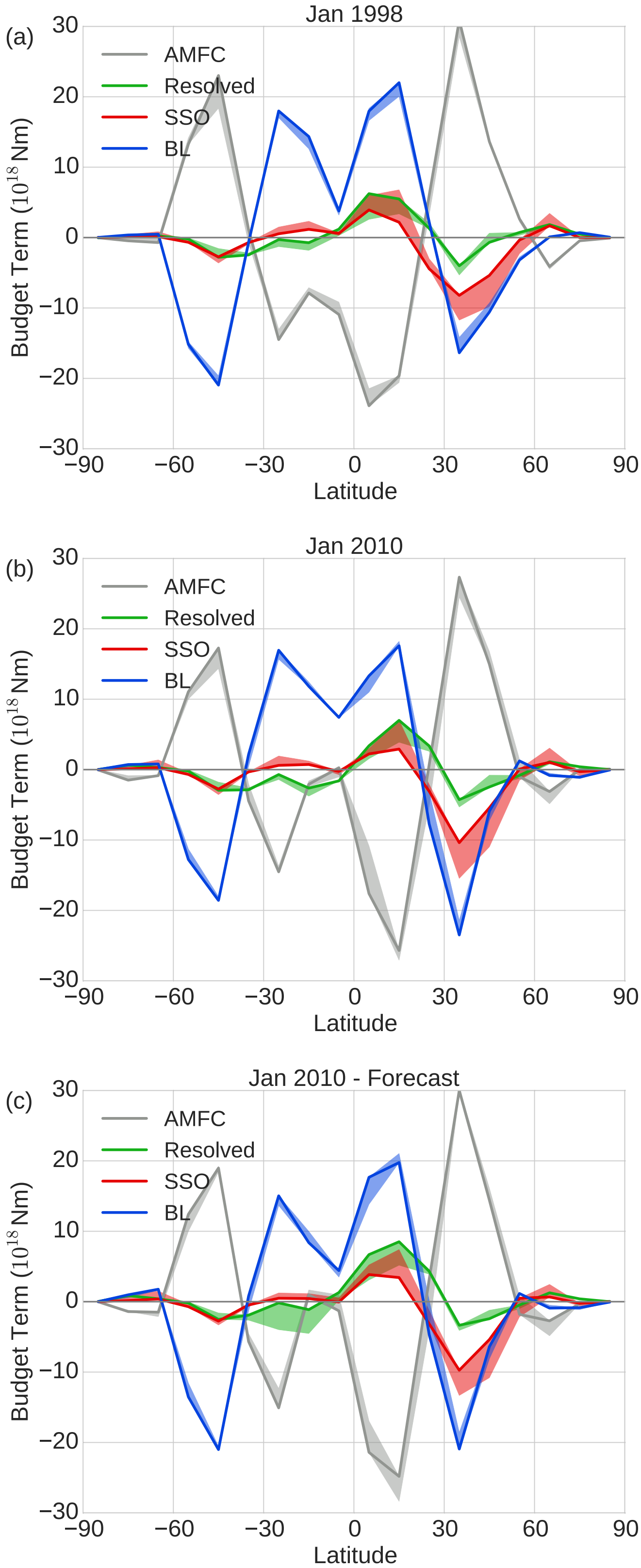

Figure 2. Dominant terms in the relative angular momentum budget (eq. 1) integrated over 10° latitude bands and averaged over the (a) January 1998, (b) January 2010 nudged experiments and (c) January 2010 short range forecast experiments. The solid line indicates the value of the N512 budget term and the shading indicates the range of the budget term over the N96, N216 and N512 resolution experiments.

torques and not the parameterized torques, since the sign of the parameterized drag depends only on the sign of the grid-box mean winds. This can be problematic for determining the correct total orographic torque in these regions, since, theoretically, either term can go to any magnitude in the opposite sign and still give the same total.

The angular momentum balance between the atmospheric torque and surface torque is larger in the NH than in the SH due to both the asymmetry of the land and the fact that in NH winter there is an enhanced midlatitude jet, which would interact strongly with the prominent orography in those regions. The torque coming from the boundary layer drag is the major contributor towards balancing the torque coming from the AMFC, since it acts over both land and ocean. Comparing the two years, there is a shift in the contributions to the budget between the boundary layer and the AMFC over the tropics in the region 0S to 20S. This may be due to the fact that January 1998 experienced a particularly strong El Niño, which would lead to redistribution of the mass in the atmosphere and, as a result, have a substantial influence on the angular momentum of both the atmosphere and the solid Earth (Chao 1988). It is interesting to note that while both the BL torque and SSO torque are substantially larger over the NH extra-tropics in January 2010 compared with January 1998, the resolved orographic torque is relatively unchanged. This provides additional evidence that the resolved torques respond differently to the surface flow than do the SSO or BL torques.

2.4. *Verification against forecasts*

As a further means of verifying our method of constraining the climatology and reducing the variability in the AMFC between experiments of different resolutions, 31 short range forecasts initialised from ECMWF analysis at 00UTC for the month of January 2010 were performed. The idea is to confirm that the sensitivity of the resolved and parameterized torques to model resolution is not somehow connected to the nudging itself. These forecast experiments were performed using the same model setup, model physics and model resolutions as with the nudging experiments. The only difference between them is that the forecasts are run with 70 model levels extending to 80km instead of 85 model levels extending to 85km, since the former is the standard global forecasting setup. Figure 2c shows the dominant terms in the angular momentum budget for the forecast experiments performed over January 2010, with the shading indicating the range over the three model resolutions as in figures 2a and 2b. Comparing the January 2010 forecast to its nudging counterpart, the overall shape of the terms are relatively similar. There are some differences between the magnitude of the extrema of the AMFC and BL torques, which may arise due to differences between ERA-interim and the operational ECMWF analysis. However, the important point for our purposes is that the sensitivity of the different terms to horizontal resolution is very similar.

3. Sensitivity to model resolution

The shape, sign and maxima of the AMFC term does not change much across the three resolutions in figure 2. Along with the fact that the lower tropospheric winds at all three resolutions adjust to the ERA-interim winds (figure 1c), the similarity in the AMFC terms is a further indication that the nudging is constraining the climatologies at the different resolutions. Since the BL drag parameterizes scales smaller than 5km, and we are not resolving those even at the highest resolution considered, the magnitude of this term sees little change between the resolutions. The parameterized SSO torque, however, varies substantially between the resolutions, most notably in the 30N to 60N and 0N to 20N regions, where it drops by more than a quarter between the N96 and N512 resolutions. Although there is an increase in the magnitude of the resolved torque to balance that of the decreasing SSO torque in the 0N to 20N region, there is very little change in the resolved torque relative to the SSO torque elsewhere. This resolution sensitivity is evident in both years shown in figure 2, as well as in the forecast experiments. Offline calculations of the blocking component of the SSO torque, when holding static stability, zonal wind and density constant across resolution, show a similar resolution sensitivity to that seen in the full model experiments (not shown). This suggests that, while static stability and zonal wind changes may play some role, it is the sub-grid orographic parameters that contribute most to the resolution sensitivity.

To further illustrate the exchange between the resolved and parameterized torques, scatter plots motivated by figure 3 in Brown (2004) of the orographic torques at different resolutions have been plotted in figures 3 and 4 for the nudged experiments. The left hand column of figures 3 and 4 compare the N96 parameterized orographic torques on the x-axis with those of the N216 and N512 resolutions' on the y-axis. The right hand column of figures 3 and 4 then compare the N96 resolved orographic torques with those of the N216 and N512 resolutions'. Each point corresponds to an instantaneous value of the torque at 6 hourly intervals for the month of January and the colours indicate the 10° latitude band considered. In most regions of the NH, the magnitude of the resolved and parameterized torques in the N96 experiments are similar, although there is much larger variability in the resolved torque while the parameterized torque is of almost constant sign for each latitude band. The dependence of the resolved torque on differential heating and synoptic scale pressure systems passing over large topography means that there is a large variation in the sign of the resolved torque on daily timescales. The parameterization schemes, however, assume only a wind direction and static stability dependence, which is why this difference in sign between the resolved and parameterized torques over certain regions exists. This variability in the resolved torque also explains why there are smaller values of the resolved torques in the monthly mean picture, despite the instantaneous magnitude of the resolved torques being larger than the SSO torques in some instances.

The slope of the scatters in figures 3a,c and 4a,c show that there is a decrease in the magnitude of the parameterized torque with increasing resolution, as would be expected. However, figures 3b,d and 4b,d do not show a corresponding increase in the resolved orographic torque and, although some exchange is seen in the latitude band between 10N to 30N, most of the points lie on the one-to-one line. This implies that there is more total orographic torque, resolved plus parameterized, at lower resolutions, particularly in the 30N to 50N region.

In the SH, the magnitude of the resolved torque is much larger than the parameterized torque, a feature that is not evident from the monthly mean budget plots. Compared to the NH, the SSO and resolved torques are also much smaller, since there is less land mass here and, although the torque from the Andes and the Antarctic Peninsula are substantial, they become diluted in the zonal mean. As in the NH, figures 3d and 4d shows that there is a one-to-one relationship between the resolved torques, indicating a lack of increased resolved orographic torque with increasing resolution.

Figures 5 and 6 show scatter plots of the orographic torques at different resolutions, as in figures 3 and 4, but now for the experiments constrained by short range forecasts. The one-to-one relationship between the resolved torque at different resolutions in the 30N to 60N region is as evident in the forecast experiments as in the nudging experiments, as is the large reduction in the parameterized torque with increasing resolution. This confirms that this resolution sensitivity is not an artefact of the nudging and is a genuine property of the model at these resolutions.

It is clear from the zonal mean scatter and momentum budget plots that each latitude responds differently to changes in resolution as a result of the circulation or orographic features

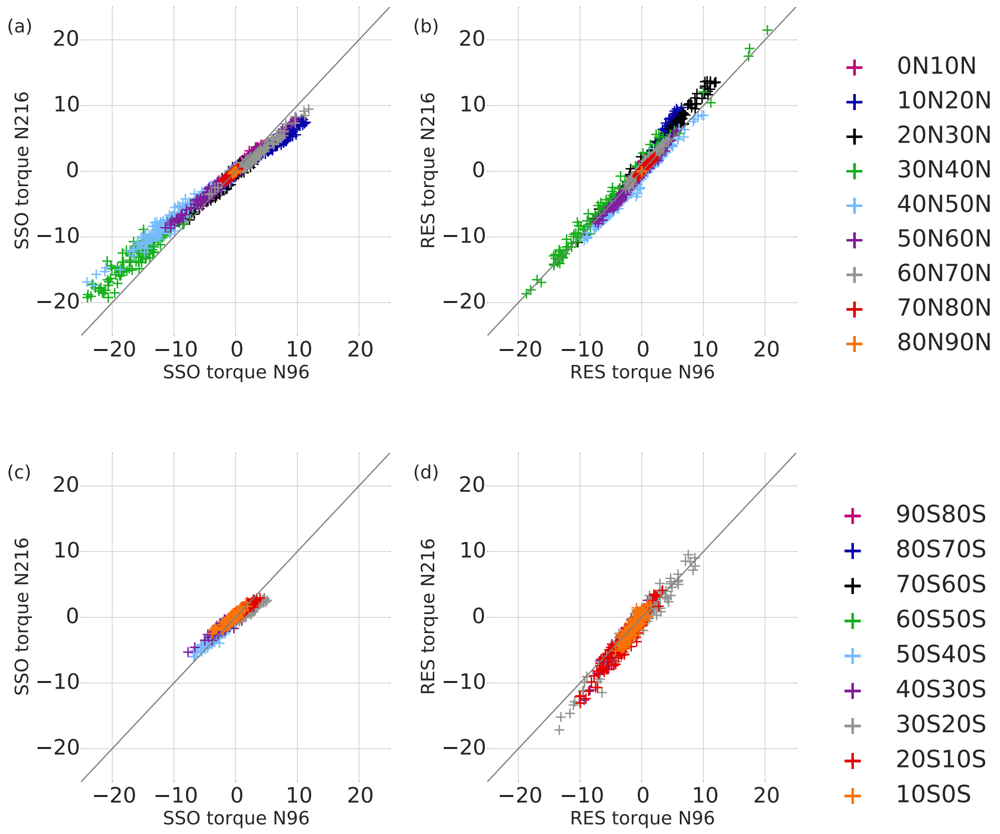

Figure 3. Scatter plots of (a),(c) sub-grid scale orographic (SSO) torques and (b),(d) resolved orographic torques for nudged experiments at resolutions N96 vs N216 for January 2010. Each point corresponds to a 6 hourly instantaneous value and colours indicate the 10° latitude band integrated over.

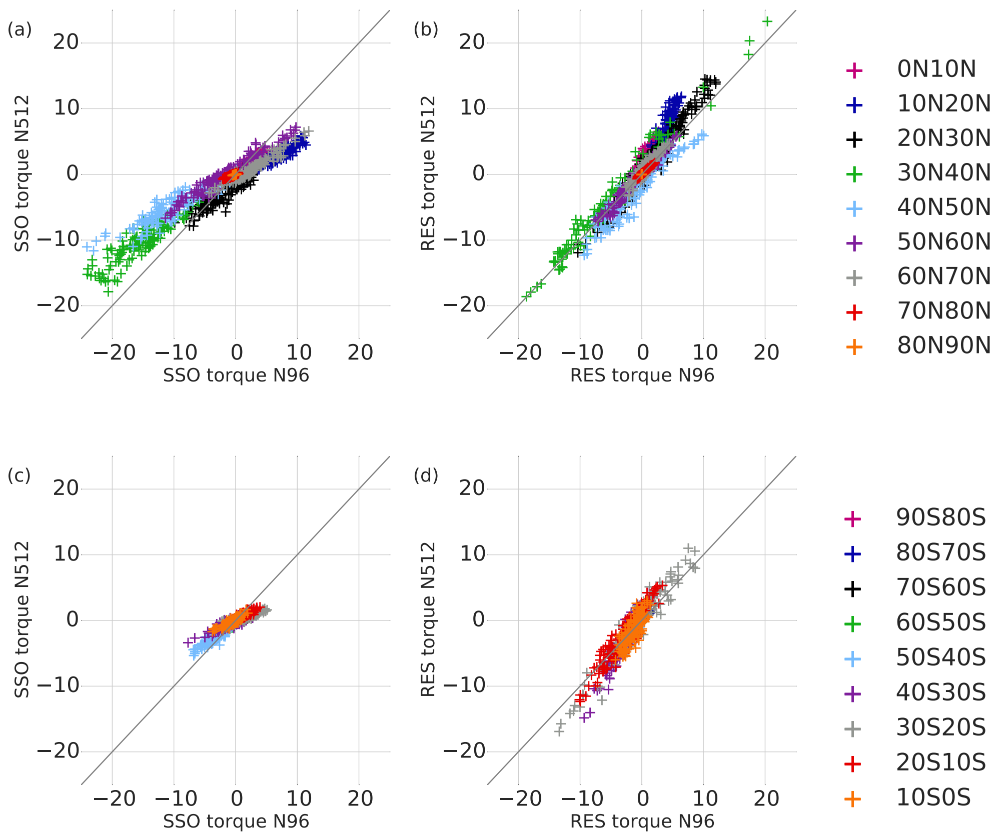

Figure 4. As in figure 3 but for resolutions N96 vs N512.

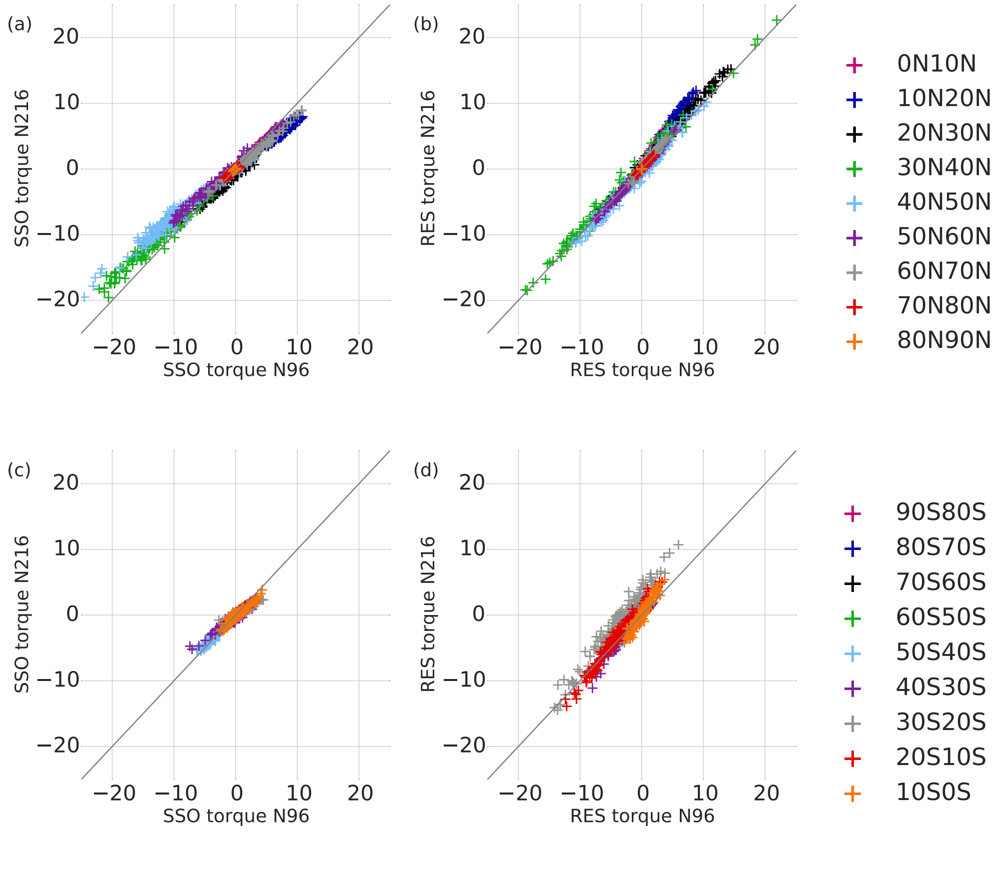

Figure 5. As in figure 3 but for the short range forecast experiments.

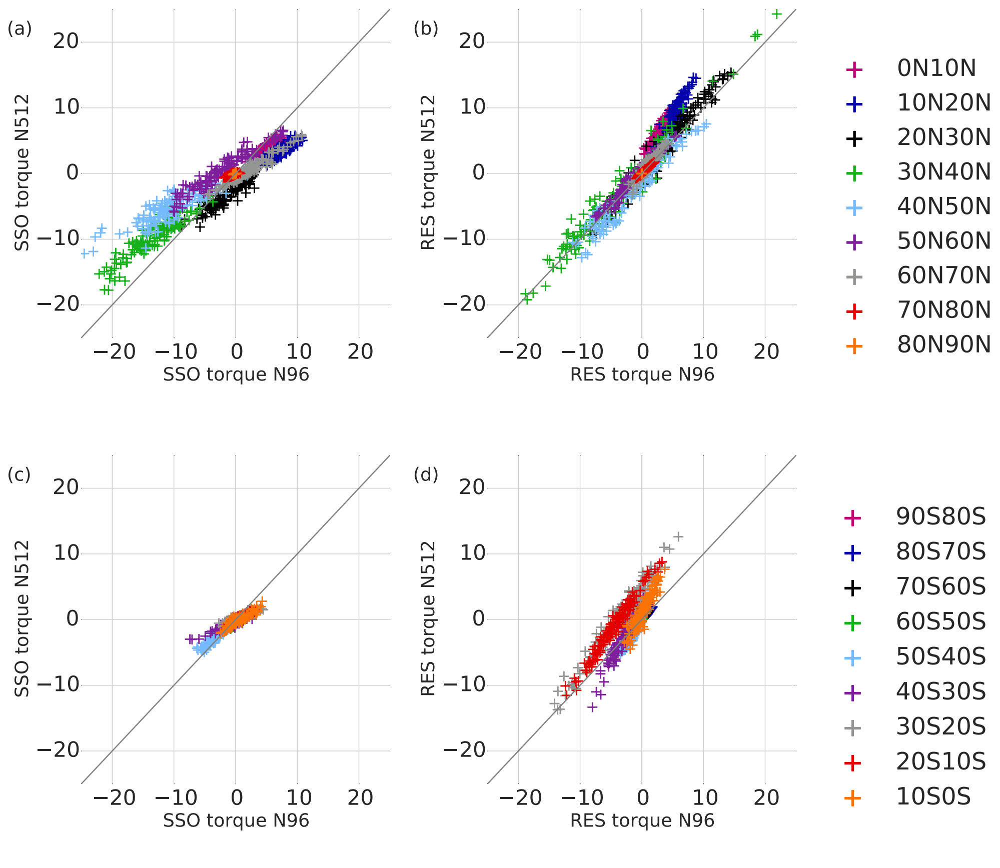

Figure 6. As in figure 5 but for resolutions N96 vs N512.

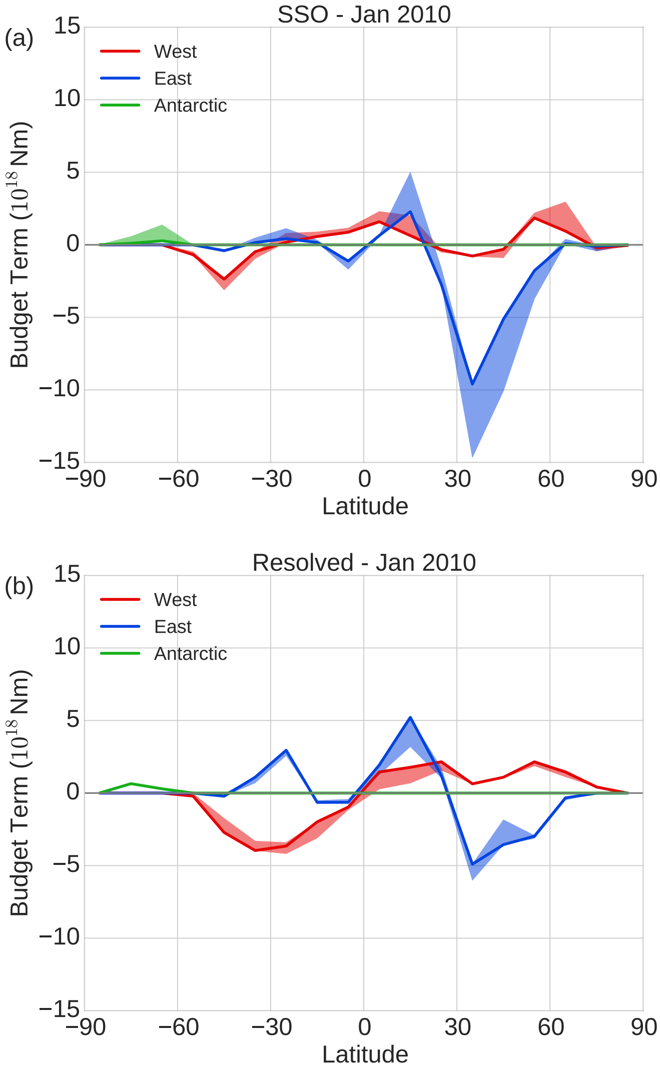

Figure 7. (a) Sub-grid scale parameterized (SSO) and (b) resolved orographic torques integrated over the Western Hemisphere (∼180 to ∼350 longitude, encompassing the Americas and Greenland), the Eastern Hemisphere (∼350 to ∼180, encompassing Eurasia and Africa) and the Antarctic, averaged over the January 2010 nudged experiment. The solid line indicates the value of the N512 experiment and the shading indicates the range over the N96, N216 and N512 resolution experiments.

in that region. Figure 7 shows the contribution to the zonal mean SSO and resolved torques integrated over the Eastern Hemisphere (from approximately 180 to 350 longitude), the Western Hemisphere (from approximately 350 to 180 longitude) and the Antarctic for the January 2010 nudged experiments. The integrations are performed over land masses so that the Eastern Hemisphere includes the entire African, Asian, European and Australian continents and the Western Hemisphere includes the Americas and Greenland. As resolution increases, there is very little change in the resolved torque over the Antarctic Peninsula, while the SSO torque reduces substantially. Similarly, the SSO torque becomes far less negative with increasing resolution over the Eastern Hemisphere between 30N to 60N, which encompasses the Alps, the Caucasus and the Himalayas, compared to the small increase seen in the resolved torque. The Western Hemisphere resolved and SSO torque are of opposite sign and do not change much with resolution over the Rockies between 20N to 40N. At lower latitudes, between approximately 0N to 20N, the change in the resolved and SSO torque across resolution is almost like-for-like over both the Western and Eastern Hemispheres. This latitudinal and longitudinal dependence of the resolution sensitivity indicates that, although the parameterized and resolved orographic torques exchange well in certain regions, the different mountain massifs respond very differently and particular attention should be paid to the Eastern Hemisphere middle latitudes.

4. Impact on model bias

Figures 8a, 8b and 8d show the total orographic torque, resolved plus parameterized, for the January 1998 and January 2010 nudged experiments and the January 2010 forecast experiments in red. Although the total torque is very similar at most latitudes, implying that the model maintains a total orographic torque across resolutions in most areas, there are certain regions where the N96 experiments have much larger orographic torque than the higher resolutions. The most prominent of these is the 30N to 60N region, where the N96 resolution has in excess of a quarter more than that of the N512 experiments. This behaviour is seen in both the nudged and the forecast experiments.

The impact of this additional torque at lower resolutions on the large scale circulation may be substantial and could lead to large systematic biases in climate models. In order to quantify the drift that would have occurred in the nudged experiments if this model were free running the tendencies output by the nudging routine are analysed, which are proportional to the differences between the model and ERA-interim at every time-step. These tendencies have been vertically integrated and represented as a torque in figures 8a and 8b in blue, with the shading again indicating the range between the model resolutions. Both years show an overall decrease in the magnitude of the nudging tendencies with increasing resolution at most latitudes, as might have been expected based on the fact that we are parameterizing less and thus prone to less parameterization error. This monotonic reduction in the nudging tendencies with increasing resolution is consistent with the climatological biases in the free running version of the MetUM, which are found to reduce in amplitude but remain similar in structure and spatial distribution across resolutions (Martin *et al.* 2010).

In both the 1998 and 2010 nudged experiments, in the 30N to 60N region where this discrepancy in the total orographic torque is persistently identified, the nudging torque is of the opposite sign to the additional orographic torque at lower resolutions. There is a striking difference in the magnitude of the nudging torque in this region between the Jan 2010 and Jan 1998 experiments, with the 2010 values being more than double those of 1998. This is consistent with the fact that the Jan 2010 experiment has both larger orographic and BL torques, which may be acting to decelerate the flow in excess and, thus, the nudging has to respond more strongly. Figure 7 identifies this model error as being likely due to the SSO torques over the Himalayas.

The drift in the forecast experiments was calculated as the difference in the vertically integrated and zonally averaged rate of change of angular momentum, $\partial[\int_{z_0}^{\infty} m\rho dz]/\partial t$, between the model and analysis over the 24 hour forecasts. This is shown in blue in figure 8d and has been multiplied by a factor of four since the scale of the drift in the forecast is much smaller than the nudging. The reason for this amplitude difference comes from the fact that the forecasts are initialised throughout the entire depth of the atmosphere, whereas the nudging is applied only in the upper atmosphere. Besides their magnitude, there are several other differences between the forecast drift and the nudging tendencies, such as the large drift seen in the tropics and the double maxima seen between 30S and 60S. The drift in the tropics does not reduce with increasing resolution, as was also seen in the nudging tendencies for January 1998. Understanding the model bias in the tropics may be much more complex than in midlatitudes as a result of diabatic processes. The focus of this study, however, is the midlatitudes where the model drift reduces with increasing resolution, particularly between 30N and 60N. This supports

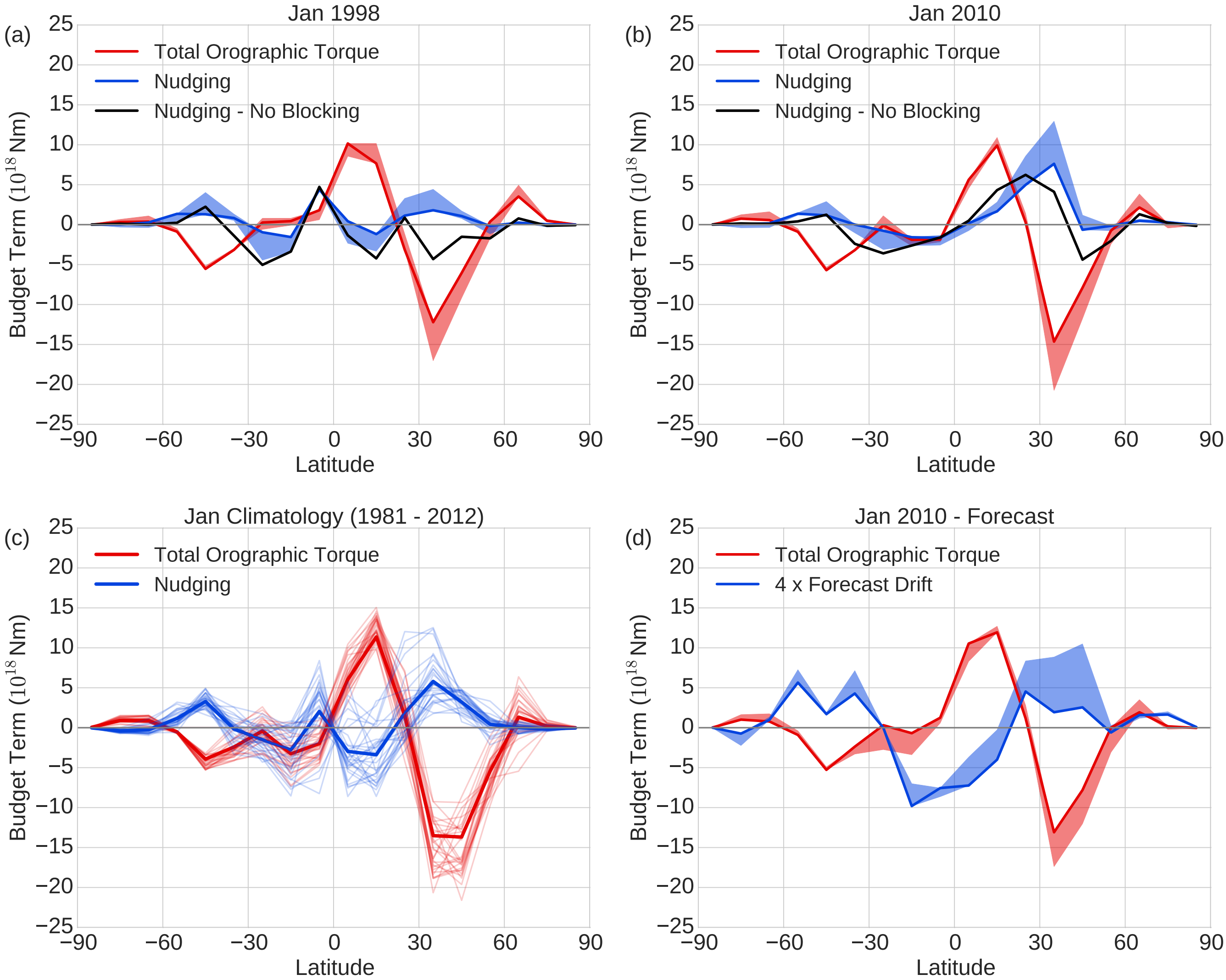

Figure 8. Vertically integrated nudging tendencies and total resolved plus parameterized orographic torque for (a) January 1998 nudged experiments, (b) January 2010 nudged experiments and (c) January climatology from 1981 to 2012. (d) shows the drift relative to the analysis in the vertically integrated angular momentum ($\times 4$) and the total orographic torque for short-range forecast experiments over January 2010. In (a), (b) and (d) the solid line indicates the value of the N512 experiment and the shading indicates the range over the N96, N216 and N512 resolution experiments. In (c) the thick line indicates the climatology and the thin lines are the individual years, at N96. The black lines in (a) and (b) indicate the nudging tendencies at N96 when the orographic blocking is set to zero (NoBLK).

the idea that excessive parameterized orographic torque at lower resolution may be leading to model bias in the NH midlatitudes.

In the assessment of nudging tendencies as an indication of the model bias, it is important that they are generally representative of the overall climatological biases in the model. By performing 32 separate experiments using the N96 setup for each January in the years 1981 to 2012, a climatology of the nudging tendencies at the N96 resolution was built. Figure 8c shows the total orographic torque for the individual Januaries from 1981 to 2012 in red and the corresponding vertically integrated nudging tendencies in blue, with the thick line indicating the mean January climatology. The positive torque from the nudging tendencies acting to accelerate the atmosphere in the region between 30N and 60N is quite robust across all of the years, with some years having very substantial values here. In addition to this easterly bias in the NH, there also appears to be a robust easterly bias in the SH midlatitude jet.

The effect of the additional parameterized torque at the N96 resolution is assessed by setting the orographic blocking term, the largest component in the SSO torque, to zero and looking at the resulting nudging tendencies, which are shown in black in figures 8a and 8b. The vertically integrated tendencies of the experiment without orographic blocking (NoBLK) are of similar magnitude and sign as those of the N96 control experiment (CNTRL) in most latitudes, apart from in this interesting 30N to 60N region, where the magnitude is substantially reduced or the sign is switched. This implies that the low level blocking parameterization can have a significant impact on the large scale circulation over the NH extra-tropics. The change in sign of the nudging tendency indicates that the parameterized blocking term is needed but is too strong. Additionally, the lack of change in the nudging tendencies at other latitudes suggests that there may be compensation by other terms in the momentum budget occurring. The compensation by other terms within the momentum budget is discussed in the following section.

5. Compensation by other terms in the momentum budget

The nudging framework employed here is ideal not only for resolution sensitivity studies but also for parameter sensitivity studies. Since the AMFC is constrained through nudging, without the torque due to orographic blocking, other terms in the momentum budget could increase or decrease in order to compensate for this. The way in which the BL torque, resolved torque and subsequently the nudging respond to this loss of orographic torque may give some insight into the suitability of using one parameterization scheme to compensate for the other and the consequences of such substitutions.

Figure 9 shows the major contributors to the zonal mean momentum budget at N96 resolution for the January 1998 and

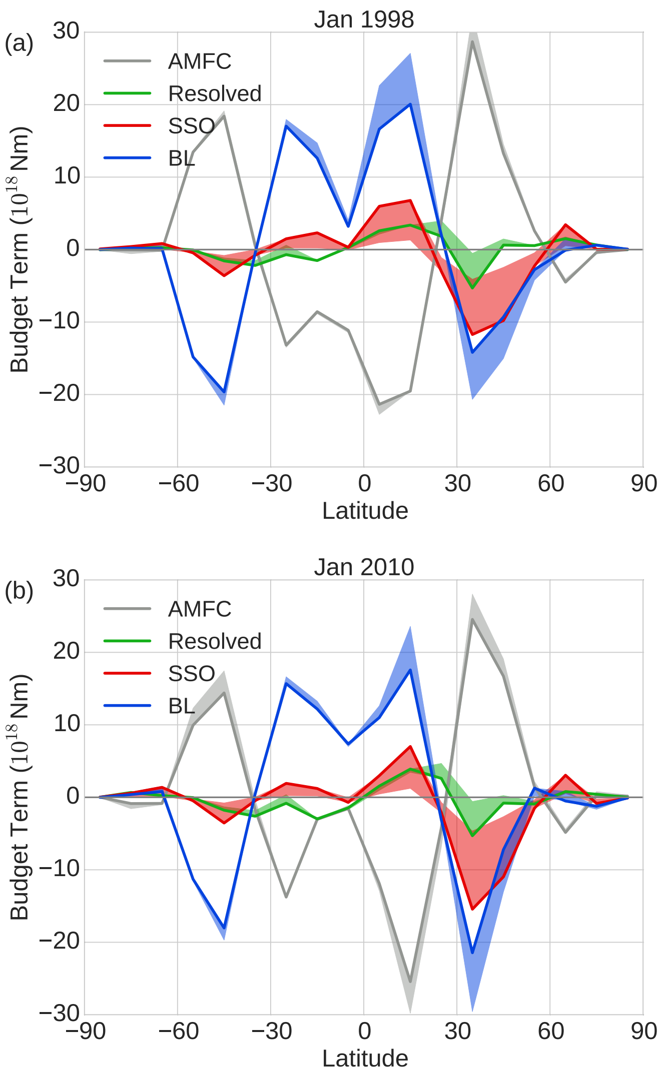

Figure 9. Dominant terms in the angular momentum budget of the N96 CNTRL experiments and N96 NoBLK experiments for (a) January 1998 and (b) January 2010 with nudging. The solid line indicates the values of the N96 CNTRL experiment and shading indicates the range of the term between the CNTRL and NoBLK experiments.

January 2010 CNTRL and NoBLK experiments. The SSO torque does not go to zero in the NoBLK experiment due to the gravity wave component of the parameterization, which was not set to zero so as to investigate its response to the loss of orographic blocking. In general there is little difference in the BL torque over the SH in figure 9 where the reduction in SSO torque leads to a decrease in the nudging tendency between 60S and 40S and a change of sign at 40S (Figures 8a and 8b). Within the 10S to 40S region the resolved torque decreases, but unlike in the NH this is a compensation since the resolved torque is of opposite sign to the SSO torque. The NH shows a strong response from the BL and resolved torques, where the loss of blocking is almost fully compensated by a combination of the two in the 0N to 30N region. However, despite the BL torque increasing substantially over the 30N to 60N region, the compensation is not large enough to account for the loss of the blocking term. What is more, the torque due to gravity wave drag increases from a negligible amount, which is indistinguishable from the zero line, to the lower edge of the shaded region in the SSO term in figures 9a and 9b. This lack of compensation from the BL torque and parameterized gravity wave torque between 30N to 60N is evident in the vertically integrated nudging tendencies (8a and 8b), where they become less positive and/or change sign.

An increase in the parameterized gravity wave drag occurs due to an increase in the local wind speed and, as a result, an increase in energy available to scale the mountain and generate gravity waves. Both the turbulent mixing (Lock *et al.* 2000) and turbulent orographic form drag (Wood and Mason 1993) component of the BL parameterization have a dependence on wind such that an increase in the local wind will lead to an increase in the total BL drag, which is why we see this compensating behaviour when the orographic blocking is switched off. One might also expect that increased winds would lead to larger pressure gradients acting on resolved orography and, as a result, larger resolved torques being exerted on the atmosphere. What is most surprising about these NoBLK experiments is that the resolved drag does not compensate for the orographic blocking between 20N to 60N and, instead, becomes more positive between 20N to 30N and less negative (or changes sign) over 30N to 50N. The change in the resolved torque acts in the same sense as the change in the SSO torque and together leads to the large decrease or change of sign seen in the nudging tendencies over this region.

As discussed in section 3, the individual mountain massifs respond differently to changes in resolution and it is now evident from figure 9 that they also respond differently to removal of the blocking parameterization. In order to identify the response of the torques over specific regions of the globe to switching off the orographic blocking, latitude/longitude plots of the change in vertically integrated momentum budget tendencies between the N96 CNTRL and NoBLK experiments are plotted in figure 10, along with their hemispheric means on the left and right hand side of each panel. The contribution from integrating over the Antarctic continent is plotted in the bottom right-hand panel. The terms have not been area weighted and are expressed as a stress (Pa), in order to expose some of the finer details at higher latitudes (According to our sign convention, these stresses are actually the negative of the surface stress as conventionally defined). Figures 10a and 10b show the change in the SSO and BL stress and figure 10c shows the sum of these changes, so as to identify where the BL stress (and gravity wave drag) does not compensate for the loss of orographic blocking. Figure 10d shows the differences in the semi-Lagrangian advection tendencies; since the AMFC is constrained by nudging, these will be predominantly due to changes in the resolved pressure torques. The sum of the change in the SSO, BL and advection term is shown in figure 10e and the change in the nudging tendencies is shown in figure 10f, note the change in scale. The similarity of figures 10e and 10f confirms that the budget is well closed. The change in the surface pressure when blocking is switched off is plotted in figure 11 along with the 850hPa wind vectors from the CNTRL experiment. Comparing figure 10a and the wind vectors in figure 11, it is evident that the sign of the parameterized stress depends on the sign of the wind.

The responses seen over individual mountain regions are summarised in table 1 by stating the sign of the term in the CNTRL experiment, the degree to which each term is able to compensate and the change seen in the nudging tendency. If the sign of the nudging is opposite to (the same as) the blocking stress in the CNTRL experiment it suggests there is excessive (insufficient) surface stress in that region in the CNTRL experiment. Where there is excessive stress and removing the orographic blocking leads to a decrease in the magnitude of the nudging, the BL and resolved stress do not compensate fully for the loss of blocking and the model bias is reduced. Where there is insufficient drag and the magnitude of the nudging tendencies increase when blocking is switched off, the BL and resolved stress do not compensate fully and now the bias is increased. Where the magnitude of the nudging tendencies remain unchanged, the resolved stress and BL stress compensate for the loss of orographic blocking. We see that over the Antarctic, the Andes and Europe, the nudging is of opposite sign to the SSO in the CNTRL, indicating excessive drag, and the bias is reduced as a

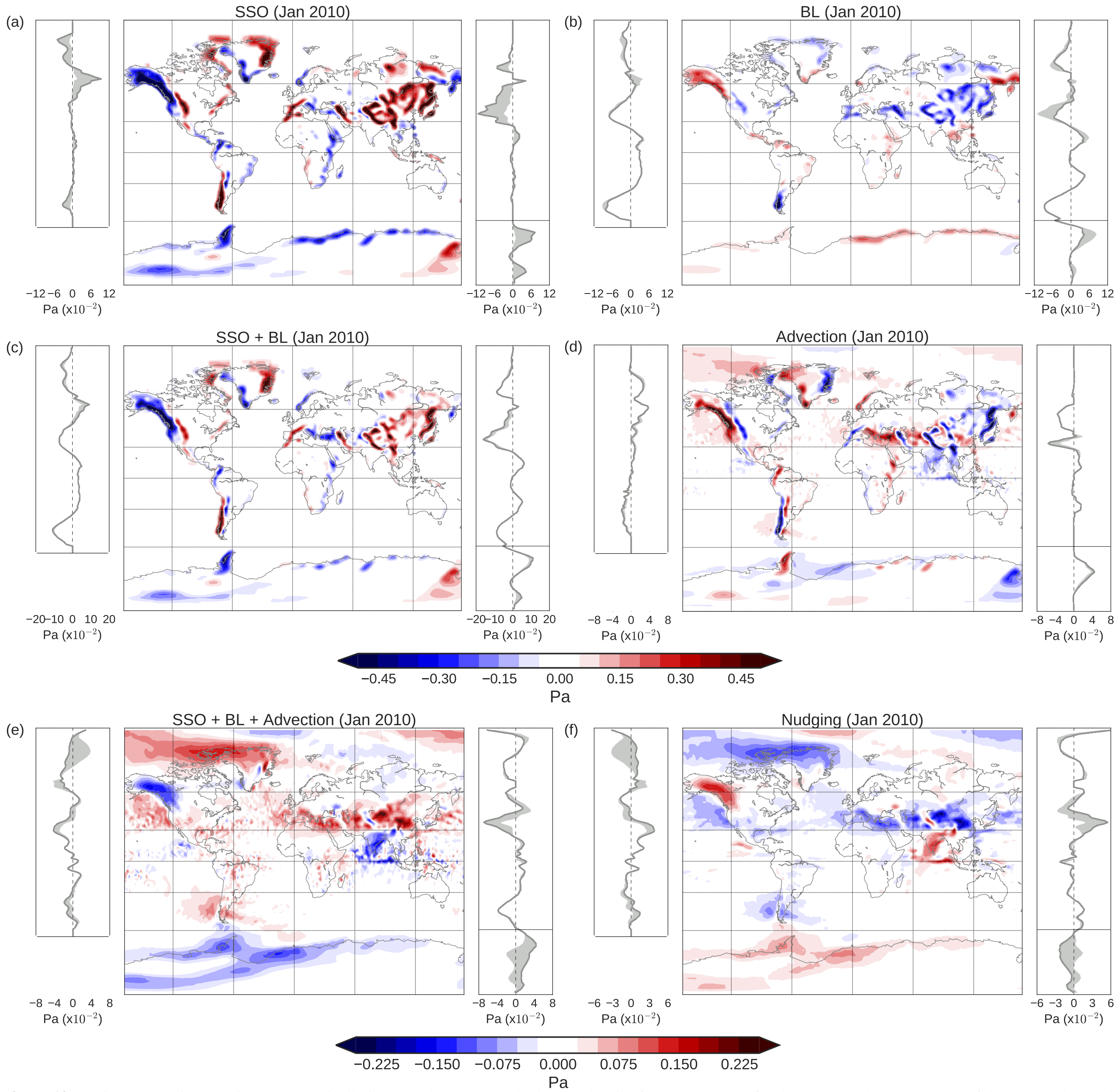

Figure 10. N96 NoBLK minus N96 CNTRL vertically integrated momentum budget tendencies for January 2010 for the (a) SSO, (b) BL, (c) sum of the SSO and BL, (d) semi-Lagrangian advection, mainly representing the resolved pressure torque, (e) sum of the SSO, BL and semi-Lagrangian advection and (f) nudging. Note the difference in scale between figures (a)-(d) and figures (e) and (f). Left and right side panels are the Western and Eastern Hemisphere zonal means, respectively. The lower right side panel is the mean over the Antarctic. The solid line indicates the values of the N96 CNTRL experiment and shading indicates the range of the term between the CNTRL and NoBLK experiments.

result of removing the parameterized blocking stress. Over East Asia, Central America and East Africa, there is little change in the nudging when blocking is removed, indicating that the BL and resolved stress compensate for the parameterized blocking over these regions. The only region over which there is insufficient drag in the CNTRL and the nudging tendencies increase in magnitude in NoBLK is over the Rockies, particularly to the North.

By far the most complex topographic region is the Himalayas and the Tibetan Plateau, which is why it is not included in table 1 and will be discussed here. The BL stress is able to compensate partially over the major regions of the Himalayas (fig. 10c) and, while the resolved stress compensates over the highest peaks (fig. 10d), the total stress reduces on the leeward side of the Himalayan mountain chain (fig. 10e), acting to reduce the drag on the westerlies in this region. Since the BL does not fully compensate for the loss of parameterized blocking and the resolved stress responds in the opposite sense to a compensation, the nudging tendencies reduce substantially or even change sign (fig. 10f).

Consistent with the large change seen in the resolved pressure torque when blocking is switched off, figure 11 shows that there is a large increase in the surface pressure on the leeward side of the Himalayan mountain chain. Similar magnitude changes can be seen over the Northern Rockies and Europe. The change in surface pressure over the NH seen in these nudged experiments match closely with the forecast experiments performed by Sandu *et al.* (2016) after a 24 hour lead time in which the orographic blocking was increased. They looked at how the surface pressure responded to increasing the blocking over specific mountain regions using short range forecasts and found that all of the changes in the surface pressure in midlatitudes at a 24 hour lead time are local responses to changes in the blocking. This indicates that the changes seen in the surface pressure and, therefore, resolved

Table 1. Sign of momentum budget terms in CNTRL experiment and response in NoBLK experiment over specific mountain regions in figure 10.

	SSO	BL	Resolved	Nudging
Antarctic	Coast/Peninsula: >0	Coast: CNTRL>0 Partial compensation	Peninsula: CNTRL >0 Strong compensation	CNTRL <0 Large decrease in magnitude
	Ross Ice Shelf: <0	Ross Ice Shelf: CNTRL ∼0 No response	Ross Ice Shelf: CNTRL <0 Full compensation	Ross Ice Shelf: CNTRL >0 Little change
Andes	<0	CNTRL <0 Large compensation in south No response in north	CNTRL <0 Partial compensation	CNTRL >0 Large decrease in magnitude
E. Africa	>0	CNTRL >0 Little compensation	CNTRL >0 Localised compensation over Ethiopia and Tanzania	CNTRL <0 Little change
C. America	>0	CNTRL >0 Little compensation	CNTRL >0 Almost full compensation	CNTRL >0 Little change
Rockies	North: >0	North: CNTRL >0 Partial compensation	North: CNTRL >0 Partial compensation	North: CNTRL >0 Increase in magnitude
	South: <0	South: CNTRL <0 Little compensation	South: CNTRL <0 Almost full compensation	South: CNTRL <0 Increase in magnitude
Europe	Alps/Caucasus: <0	Alps: CNTRL <0 Little response Caucasus: CNTRL <0 Partial compensation	Alps/Caucasus: CNTRL <0 Almost full compensation	Everywhere: CNTRL >0 Large decrease in magnitude
	Turkey/Croatia: >0	Turkey: CNTRL <0 Compensation of opposite sign	Turkey: CNTRL >0 Increase in magnitude in response to BL	
E. Asia	<0	CNTRL >0 Change in sign for partial compensation	CNTRL <0 Full compensation	CNTRL ∼0 Little change

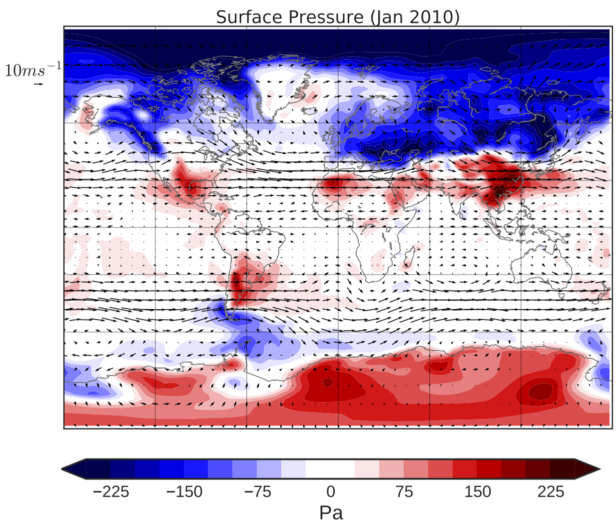

Figure 11. Difference in the surface pressure between the N96 CNTRL and N96 NoBLK nudged experiments, vectors are 850hPa wind for CNTRL.

pressure torques in the nudged experiments are also tied to the specific topographic features.

6. Conclusions

The sensitivity of resolved and parameterized orographic torques to changes in model resolution and parameterization within the Met Office Unified Model was investigated in the context of the angular momentum budget. The methods employed in this study demonstrate that nudging techniques can be fruitful in diagnosing errors in the parameterized surface stresses and have illuminated the impact that orographic parameterization schemes have at lower (climate) horizontal resolutions. By nudging the MetUM towards ERA-interim within the regions of maximum momentum flux convergence in the free atmosphere, we were able to constrain the angular momentum flux convergence term within the momentum budget across model resolutions and reproduce the ERA-interim low level winds. The boundary layer torque did not change substantially across resolutions, while the parameterized orographic torque (SSO) saw the largest change. Although there was good agreement in the total orographic torques at varying resolutions in most regions, there was a large discrepancy over the 30N to 60N region. This difference is attributed to the additional parameterized orographic torque at the lower resolutions, which is not balanced by a decrease in the resolved torque. Deconstructing the zonal mean SSO torque and resolved torque into their Eastern and Western Hemispheric contributions, it was shown that the resolution sensitivity of the SSO torque came largely from the Eastern Hemisphere. This resolution sensitivity was validated using short range forecasts, which were shown to support the orographic torque resolution sensitivity in our nudged experiments.

Tendencies from the nudging routine corroborate the findings of Brown (2004) who suggest that the parameterized orographic torque within the 30N to 60N region at lower resolutions may be excessive. This was done using the ECMWF forecast model of the time, which is a completely different model to the MetUM but was run at resolutions comparable to those used here. The vertically integrated nudging tendencies in this study exhibited a tendency towards accelerating the atmospheric flow in the NH in the region where the parameterized orographic torque (which acts as a drag) is the largest. The magnitude of the nudging tendencies reduced as the parameterized torque reduced within this region when the resolution was increased, indicating that it may be the additional parameterized orographic torque that is the cause of the larger model error at lower resolution. The drift over 24 hours in short range forecasts also showed that the forecast winds were too weak in the 30N to 60N region, with this drift decreasing with increasing resolution. What is more, the climatological nudging tendencies show a large acceleration of the atmosphere at the low resolution within both the NH and SH jets, which suggests this could be linked to a robust model bias. Previous studies have shown that many systematic biases in climate models develop over short timescales and, since these errors remain local over these timescales, the analysis of nudging tendencies within constrained models can provide a means of understanding the origins of these biases (Ma *et al.* 2014).

The resolved orographic torque may be insensitive to model resolution in the regions over the Himalayas and the Rockies at the resolutions considered in this study due to the large scale nature of these features. If the large scales were dominating at these resolutions, there may not be an increase in the resolved drag until a resolution is reached in which additional small scale processes can be represented. Power spectra of the resolved pressure drag over East Africa and the Himalayas (not shown) indicate that the model does respond to changes in resolution, since there is additional small scale variance when going to higher resolution. However, the peak of the power spectrum over the Himalayas is at much larger scales, which are already well represented at N96, whereas the peak of the power spectrum over East Africa occurs at smaller scales. This explains why we see little additional resolved drag over 30N to 50N, but an increase in resolved drag over 10N to 20N, when going to higher resolutions. This may also explain why the parameterization scheme does not perform well over the Himalayas at the lower resolutions, since the large sub-grid scale mountains that are fed into the parameterizations at lower resolutions may not be suited to parameter choices made when optimising the schemes for results at higher resolutions. The lack of a scale separation in the orographic spectrum makes the modelling of orographic effects a challenge in seamless modelling and validation. Further work is required to fully understand the behaviour of the flow in the presence of orography with increasing horizontal resolution.

The blocking component of the orographic drag parameterization scheme was switched off so that the sensitivity of the nudging tendencies and other terms within the momentum budget to this parameterization may be investigated. Whilst in most regions the zonal mean nudging tendencies were similar to that of the N96 control experiment when blocking was switched off, a large change was seen over the 20N to 60N region in both the January 1998 and 2010 experiments. A lack of change in the nudging tendencies elsewhere indicated that there must be compensation by other terms in the momentum budget when the blocking is switched off. Zonal mean responses of each term within the momentum budget to the loss of orographic blocking suggests that it is predominantly the BL torque that compensates in most regions, although the resolved torques did aid the compensation to some extent. The resolved torques were found to compensate in the opposite sense to that of the SSO torques over the 20N to 30N region, however, and the BL response was found to be incomplete over this region, leading to a decrease or a change in sign of the positive nudging tendencies.

Global maps of the latitudinal and longitudinal distribution of the change in the various terms in the momentum budget in response to switching off the orographic blocking parameterization show that, while a combination of the resolved and BL stresses compensate for the orographic blocking in many regions, they can also yield an opposite response. The complex mixture of positive and negative stress over Eurasia between 20N to 40N coming from the BL, SSO and resolved stress lead to an overall decrease in the zonal mean drag over this region. This large change can be attributed to a change in the surface pressure on the leeward side of the Himalayas and an overall strengthening of the meridional pressure gradient to the north of the Eurasian mountain chain along 20N to 60N, which is also seen in the experiments of Sandu *et al.* (2016). The response of the resolved torque to variations in the strength of the sub-grid scale orographic torque raises questions in regards to the feedbacks between resolved and parameterized orographic processes. It is also clear that a substitution of the BL parameterization for the orographic blocking parameterization is not suitable in all regions. Overall, we see that the behaviour of the resolved and parameterized surface drag does not agree over the Himalayan region, which indicates that the parameterized component may not be dealing with this complex topography and atmospheric flow in a realistic manner at climate model resolutions.

Acknowledgement

This study is supported by the “Understanding the atmospheric circulation response to climate change” (ACRCC, ERC Advanced Grant) project. The authors would like to thank Miguel Teixeira for helpful discussions and John Scinocca for providing useful comments.

References

Beljaars ACM, Brown AR, Wood N. 2004. A new parametrization of turbulent orographic form drag. *Q. J. R. Meteorol. Soc.* **130**(599): 1327–1347, doi: 10.1256/qj.03.73.

Brayshaw DJ, Hoskins B, Blackburn M. 2009. The Basic Ingredients of the North Atlantic Storm Track. Part I: LandSea Contrast and Orography. *J. Atmos. Sci.* **66**(9): 2539–2558, doi:10.1175/2009JAS3078.1.

Brown AR. 2004. Resolution dependence of orographic torques. *Q. J. R. Meteorol. Soc.* **130**(603): 3029–3046, doi:10.1256/qj.04.21.

Carissimo BC, Pierrehumbert RT, Pham HL. 1988. An Estimate of Mountain Drag during ALPEX for Comparison with Numerical Models. *J. Atmos. Sci.* **45**(13): 1949–1960, doi:10.1175/1520-0469(1988)045⟨1949:AEOMDD⟩2.0.CO;2.

Chao BF. 1988. Correlation of interannual length-of-day variation with El Niño/Southern Oscillation, 19721986. *J. Geophys. Res.* **93**(B7): 7709, doi: 10.1029/JB093iB07p07709.

Clark TL, Miller MJ. 1991. Pressure drag and momentum fluxes due to the Alps. II: Representation in large-scale atmospheric models. *Q. J. R. Meteorol. Soc.* **117**(499): 527–552, doi:10.1002/qj.49711749906.

Davies T, Cullen MJP, Malcolm AJ, Mawson MH, Staniforth A, White AA, Wood N. 2005. A new dynamical core for the Met Office's global and regional modelling of the atmosphere. *Q. J. R. Meteorol. Soc.* **131**(608): 1759–1782, doi:10.1256/qj.04.101.

Dee DP, Uppala SM, Simmons AJ, Berrisford P, Poli P, Kobayashi S, Andrae U, Balmaseda MA, Balsamo G, Bauer P, Bechtold P, Beljaars ACM, van de Berg L, Bidlot J, Bormann N, Delsol C, Dragani R, Fuentes M, Geer AJ, Haimberger L, Healy SB, Hersbach H, Hólm EV, Isaksen L, Kållberg P, Köhler M, Matricardi M, McNally AP, Monge-Sanz BM, Morcrette JJ, Park BK, Peubey C, de Rosnay P, Tavolato C, Thépaut JN, Vitart F. 2011. The ERA-Interim reanalysis: configuration and performance of the data assimilation system. *Q. J. R. Meteorol. Soc.* **137**(656): 553–597, doi: 10.1002/qj.828.

Diamantakis M, Davies T, Wood N. 2007. An iterative time-stepping scheme for the Met Office's semi-implicit semi-Lagrangian non-hydrostatic model. *Q. J. R. Meteorol. Soc.* **133**(625): 997–1011, doi:10.1002/qj.59.

Hartmann DL. 2007. The Atmospheric General Circulation and its Variability. *J. Meteorol. Soc. Japan* **85B**: 123–143.

Haynes PH, Marks CJ, McIntyre ME, Shepherd TG, Shine KP. 1991. On the Downward Control of Extratropical Diabatic Circulations by Eddy-Induced Mean Zonal Forces. *J. Atmos. Sci.* **48**(4): 651–678, doi:10.1175/1520-0469(1991)048⟨0651:OTCOED⟩2.0.CO;2.

Hitchcock P, Haynes PH. 2014. Zonally Symmetric Adjustment in the Presence of Artificial Relaxation. *J. Atmos. Sci.* **71**(11): 4349–4368, doi: 10.1175/JAS-D-14-0013.1.

Hoskins B, Fonseca R, Blackburn M, Jung T. 2012. Relaxing the Tropics to an observed state: analysis using a simple baroclinic model. *Q. J. R. Meteorol. Soc.* **138**(667): 1618–1626, doi:10.1002/qj.1881.

Huang HP, Sardeshmukh PD, Weickmann KM. 1999. The balance of global angular momentum in a long-term atmospheric data set. *J. Geophys. Res.* **104**(D2): 2031, doi:10.1029/1998JD200068.

Huang HP, Weickmann KM. 2008. On the Computation of the Mountain Torque from Gridded Global Datasets. *Mon. Weather Rev.* **136**(10): 4005–4009, doi:10.1175/2008MWR2359.1.

Jung T. 2011. Diagnosing remote origins of forecast error: relaxation versus 4D-Var data-assimilation experiments. *Q. J. R. Meteorol. Soc.* **137**(656): 598–606, doi:10.1002/qj.781.

Kim YJ, Doyle JD. 2005. Extension of an orographic-drag parametrization scheme to incorporate orographic anisotropy and flow blocking. *Q. J. R. Meteorol. Soc.* **131**(609): 1893–1921, doi:10.1256/qj.04.160.

Klinker E, Sardeshmukh PD. 1992. The Diagnosis of Mechanical Dissipation in the Atmosphere from Large-Scale Balance Requirements. *J. Atmos. Sci.* **49**(7): 608–627, doi:10.1175/1520-0469(1992)049⟨0608:TDOMDI⟩2.0.CO;2.

Lock AP, Brown AR, Bush MR, Martin GM, Smith RNB. 2000. A New Boundary Layer Mixing Scheme. Part I: Scheme Description and Single-Column Model Tests. *Mon. Weather Rev.* **128**(9): 3187–3199, doi:10.1175/1520-0493(2000)128⟨3187:ANBLMS⟩2.0.CO;2.

Lott F, Miller MJ. 1997. A new subgrid-scale orographic drag parametrization: Its formulation and testing. *Q. J. R. Meteorol. Soc.* **123**(537): 101–127, doi:10.1002/qj.49712353704.

Ma HY, Xie S, Klein SA, Williams KD, Boyle JS, Bony S, Douville H, Fermepin S, Medeiros B, Tyteca S, Watanabe M, Williamson D. 2014. On the Correspondence between Mean Forecast Errors and Climate Errors in CMIP5 Models. *J. Clim.* **27**(4): 1781–1798, doi:10.1175/JCLI-D-13-00474.1.

Martin GM, Milton SF, Senior CA, Brooks ME, Ineson S, Reichler T, Kim J. 2010. Analysis and Reduction of Systematic Errors through a Seamless Approach to Modeling Weather and Climate. *J. Clim.* **23**(22): 5933–5957, doi:10.1175/2010JCLI3541.1.

McFarlane NA. 1987. The Effect of Orographically Excited Gravity Wave Drag on the General Circulation of the Lower Stratosphere and Troposphere. doi:10.1175/1520-0469(1987)044⟨1775:TEOOEG⟩2.0.CO;2.

McLandress C, Scinocca JF, Shepherd TG, Reader MC, Manney GL. 2013. Dynamical Control of the Mesosphere by Orographic and Nonorographic Gravity Wave Drag during the Extended Northern Winters of 2006 and 2009. *J. Atmos. Sci.* **70**(7): 2152–2169, doi:10.1175/JAS-D-12-0297.1.

Miller MJ, Palmer TN, Swinbank R. 1989. Parametrization and influence of subgridscale orography in general circulation and numerical weather prediction models. *Meteorol. Atmos. Phys.* **40**(1-3): 84–109, doi:10.1007/BF01027469.

Nappo CJ. 2002. 9 Data analyses and numerical methods. *Int. Geophys. Ser.* : 209–235doi:10.1016/S0074-6142(02)80277-7.

Palmer TN, Shutts GJ, Swinbank R. 1986. Alleviation of a systematic westerly bias in general circulation and numerical weather prediction models through an orographic gravity wave drag parametrization. *Q. J. R. Meteorol. Soc.* **112**(474): 1001–1039, doi:10.1002/qj.49711247406.

Phillips TJ, Potter GL, Williamson DL, Cederwall RT, Boyle JS, Fiorino M, Hnilo JJ, Olson JG, Xie S, Yio JJ. 2004. Evaluating Parameterizations in General Circulation Models: Climate Simulation Meets Weather Prediction. *Bull. Am. Meteorol. Soc.* **85**(12): 1903–1915, doi:10.1175/BAMS-85-12-1903.

Pope V, Stratton R. 2002. The processes governing horizontal resolution sensitivity in a climate model. *Clim. Dyn.* **19**(3-4): 211–236, doi:10.1007/s00382-001-0222-8.

Sandu I, Bechtold P, Beljaars A, Bozzo A, Pithan F, Shepherdx TG, Zadra A. 2016. Impacts of parameterized orographic drag on the Northern Hemisphere winter circulation. *J. Adv. Model. Earth Syst.* **7**: n/a–n/a, doi:10.1002/2015MS000564.

Scinocca JF, McFarlane NA. 2000. The parametrization of drag induced by stratified flow over anisotropic orography. *Q. J. R. Meteorol. Soc.* **126**(568): 2353–2393, doi:10.1002/qj.49712656802.

Shepherd TG. 2014. Atmospheric circulation as a source of uncertainty in climate change projections. *Nat. Geosci.* **7**(10): 703–708, doi:10.1038/ngeo2253.

Shepherd TG, Plummer DA, Scinocca JF, Hegglin MI, Fioletov VE, Reader MC, Remsberg E, von Clarmann T, Wang HJ. 2014. Reconciliation of halogen-induced ozone loss with the total-column ozone record. *Nat. Geosci.* **7**(6): 443–449, doi:10.1038/ngeo2155.

Sigmond M, Scinocca JF. 2010. The Influence of the Basic State on the Northern Hemisphere Circulation Response to Climate Change. *J. Clim.* **23**(6): 1434–1446, doi:10.1175/2009JCLI3167.1.

Smith RB. 1979. Some Aspects of the Quasi-Geostrophic Flow over Mountains. *J. Atmos. Sci.* **36**(12): 2385–2393, doi:10.1175/1520-0469(1979)036⟨2385:SAOTQG⟩2.0.CO;2.

Smith SA, Doyle JD, Brown AR, Webster S. 2006. Sensitivity of resolved mountain drag to model resolution for MAP case-studies. *Q. J. R. Meteorol. Soc.* **132**(618): 1467–1487, doi:10.1256/qj.05.67.

Stein J. 1992. Investigation of the Regime Diagram of Hydrostatic Flow over a Mountain with a Primitive Equation Model. Part I: Two-Dimensional Flows. *Mon. Weather Rev.* **120**(12): 2962–2976, doi:10.1175/1520-0493(1992)120⟨2962:IOTRDO⟩2.0.CO;2.

Teixeira MAC. 2014. The physics of orographic gravity wave drag. *Front. Phys.* **2**, doi:10.3389/fphy.2014.00043.

Telford PJ, Braesicke P, Morgenstern O, Pyle JA. 2007. Technical Note: Description and assessment of a nudged version of the new dynamics Unified Model. *Atmos. Chem. Phys. Discuss.* **7**(6): 17 261–17 297, doi:10.5194/acpd-7-17261-2007.

van Aalst MK, Lelieveld J, Steil B, Brühl C, Jöckel P, Giorgetta MA, Roelofs GJ. 2005. Stratospheric temperatures and tracer transport in a nudged 4-year middle atmosphere GCM simulation. *Atmos. Chem. Phys. Discuss.* **5**(1): 961–1006, doi:10.5194/acpd-5-961-2005.

von Storch H, Langenberg H, Feser F. 2000. A Spectral Nudging Technique for Dynamical Downscaling Purposes. *Mon. Weather Rev.* **128**(10): 3664–3673, doi:10.1175/1520-0493(2000)128⟨3664:ASNTFD⟩2.0.CO;2.

Vosper SB. 2015. Mountain waves and wakes generated by South Georgia: implications for drag parametrization. *Q. J. R. Meteorol. Soc.* **141**(692): 2813–2827, doi:10.1002/qj.2566.

Waldron KM, Paegle J, Horel JD. 1996. Sensitivity of a Spectrally Filtered and Nudged Limited-Area Model to Outer Model Options. *Mon. Weather Rev.* **124**(3): 529–547, doi:10.1175/1520-0493(1996)124⟨0529:SOASFA⟩2.0.CO;2.

Webster S, Brown AR, Cameron DR, Jones C. 2003. Improvements to the representation of orography in the Met Office Unified Model. *Q. J. R. Meteorol. Soc.* **129**(591): 1989–2010, doi:10.1256/qj.02.133.

Wells H, Vosper SB, Yan X. 2011. An assessment of a mountain-wave parametrization scheme using satellite observations of stratospheric gravity waves. *Q. J. R. Meteorol. Soc.* **137**(656): 819–828, doi:10.1002/qj.790.

Wood N, Brown AR, Hewer FE. 2001. Parametrizing the effects of orography on the boundary layer: An alternative to effective roughness lengths. *Q. J. R. Meteorol. Soc.* **127**(573): 759–777, doi:10.1002/qj.49712757303.

Wood N, Mason P. 1993. The Pressure force induced by neutral, turbulent flow over hills. *Q. J. R. Meteorol. Soc.* **119**(514): 1233–1267, doi:10.1002/qj.49711951402.

Zadra A, Bacmeister J, Bouyssel F, Brown A, Lock A, Figueroa SN, Innocentini V, Nakagawa M, Roff G, Tolstykh M. 2013. WGNE Drag Project: http://collaboration.cmc.ec.gc.ca/science/rpn/drag_project/ .

